# An improved low-optical-power variable focus lens with a large aperture

**Lihui Wang,[1,*] Hiromasa Oku,[2] and Masatoshi Ishikawa[1,3]**

[1] *Department of Creative Informatics, Graduate School of Information Science and Technology, University of Tokyo, 7-3-1 Hongo, Bunkyo-ku, Tokyo 113-8656, Japan*

[2] *Department of Electronics and Informatics, School of Science and Technology, Gunma University, Tenjincho 1-5-1, Kiryu, Gunma pref. 376-8515, Japan*

[3] *Department of Information Physics and Computing, Graduate School of Information Science and Technology, University of Tokyo, 7-3-1 Hongo, Bunkyo-ku, Tokyo 113-8656, Japan*

[*] *wang_lihui@ipc.i.u-tokyo.ac.jp*

**Abstract:** We report an improved method of fabricating a variable focus lens in which an in-plane pretension force is applied to a membrane. This method realized a lens with a large optical aperture and high performance in a low-optical-power region. The method was verified by comparing membranes in a simulation using the finite element method. A prototype with a 26 mm-diameter aperture was fabricated, and the wavefront behavior was measured by using a Shack-Hartmann sensor. Thanks to the in-plane pretension force, the lens achieved an infinite focal length with a wavefront error of 105.1 nm root mean square.



**OCIS codes:** (220.0220) Optical design and fabrication; (220.1080) Active or adaptive optics; (080.2740) Geometric optical design; (080.3620) Lens system design.

## References and links

1. H. Ren and S.-T. Wu, *Introduction to Adaptive Lenses* (John Wiley & Sons, 2012).
2. D. Graham-Rowe, "Liquid lenses make a splash," Nat. Photonics 2–4 (2006).
3. X. Zeng and H. Jiang, "Liquid tunable microlenses based on MEMS techniques," J. Phys. D Appl. Phys. **46**(32), 323001 (2013).
4. D.-Y. Zhang, V. Lien, Y. Berdichevsky, J. Choi, and Y.-H. Lo, "Fluidic adaptive lens with high focal length tunability," Appl. Phys. Lett. **82**(19), 3171 (2003).
5. H. Oku, K. Hashimoto, and M. Ishikawa, "Variable-focus lens with 1-kHz bandwidth," Opt. Express **12**(10), 2138–2149 (2004).
6. H. Ren, D. Fox, P. A. Anderson, B. Wu, and S.-T. Wu, "Tunable-focus liquid lens controlled using a servo motor," Opt. Express **14**(18), 8031–8036 (2006).
7. N. Sugiura and S. Morita, "Variable-focus liquid-filled optical lens," Appl. Opt. **32**(22), 4181–4186 (1993).
8. H. Oku and M. Ishikawa, "High-speed liquid lens with 2 ms response and 80.3 nm root-mean-square wavefront error," Appl. Phys. Lett. **94**(22), 221108 (2009).
9. S. Xu, Y. Liu, H. Ren, and S.-T. Wu, "A novel adaptive mechanical-wetting lens for visible and near infrared imaging," Opt. Express **18**(12), 12430–12435 (2010).
10. L. Wang, H. Oku, and M. Ishikawa, "Variable-focus lens with 30 mm optical aperture based on liquid–membrane–liquid structure," Appl. Phys. Lett. **102**(13), 131111 (2013).
11. B. Berge and J. Peseux, "Variable focal lens controlled by an external voltage: An application of electrowetting," Eur. Phys. J. E **3**(2), 159–163 (2000).
12. C.-C. Cheng and J. A. Yeh, "Dielectrically actuated liquid lens," Opt. Express **15**(12), 7140–7145 (2007).
13. S. Xu, H. Ren, and S.-T. Wu, "Dielectrophoretically tunable optofluidic devices," J. Phys. D Appl. Phys. **46**(48), 483001 (2013).
14. S. Sato, "Liquid-Crystal Lens-Cells with Variable Focal Length," Jpn. J. Appl. Phys. **18**(9), 1679–1684 (1979).
15. P. Waibel, D. Mader, P. Liebetraut, H. Zappe, and A. Seifert, "Chromatic aberration control for tunable all-silicone membrane microlenses," Opt. Express **19**(19), 18584–18592 (2011).
16. C. U. Murade, J. M. Oh, D. van den Ende, and F. Mugele, "Electrowetting driven optical switch and tunable aperture," Opt. Express **19**(16), 15525–15531 (2011).
17. Y. H. Lin and H. S. Chen, "Electrically tunable-focusing and polarizer-free liquid crystal lenses for ophthalmic applications," Opt. Express **21**(8), 9428–9436 (2013).
18. H. Oku and M. Ishikawa, "High-speed liquid lens for computer vision," in 2010 IEEE Int. Conf. Robot. Autom., (IEEE, 2010).
19. M. Ye, B. Wang, M. Uchida, S. Yanase, S. Takahashi, and S. Sato, "Focus tuning by liquid crystal lens in imaging system," Appl. Opt. **51**(31), 7630–7635 (2012).

#214843 - $15.00 USD Received 26 Jun 2014; revised 27 Jul 2014; accepted 27 Jul 2014; published 5 Aug 2014

20. H. Ren and S.-T. Wu, "Variable-focus liquid lens by changing aperture," Appl. Phys. Lett. **86**(21), 211107 (2005).
21. S. Kuiper and B. H. W. Hendriks, "Variable-focus liquid lens for miniature cameras," Appl. Phys. Lett. **85**(7), 1128 (2004).
22. M. Sheploak and J. Dugundji, "Large Deflections of Clamped Circular Plates Under Initial Tension and Transitions to Membrane Behavior," J. Appl. Mech. **65**(1), 107 (1998).
23. F. Zhao, "Nonlinear solutions for circular membranes and thin plates," in SPIE Proc. **6926**, (2008).
24. C. Li, G. Hall, X. Zeng, D. Zhu, K. Eliceiri, and H. Jiang, "Three-dimensional surface profiling and optical characterization of liquid microlens using a Shack-Hartmann wave front sensor," Appl. Phys. Lett. **98**(17), 171104 (2011).
25. V. N. Mahajan, "Strehl ratio for primary aberrations: some analytical results for circular and annular pupils," J. Opt. Soc. Am. **72**(9), 1258 (1982).

## 1. Introduction

To realize focus shifting with traditional lenses, which are made of solid materials and have fixed optical properties, two or more lenses cooperate with each other. Instead of moving the solid lenses mechanically to change the focal length, a variable focus lens can dynamically control its focal length by using a single lens cell. Variable focus lenses are regarded as an innovation in the field of optics [1–3]. Many prototypes have been reported [4–15], and a number of potential applications have been proposed [9,3,16–21].

Liquid-filled variable focus lenses are based on physical deformation of the refractive surfaces, which changes their curvature. Examples include liquid–air lenses [4–7], which are capable of high response speed and high optical performance. However, if this kind of lens is oriented vertically and its aperture is large, the lens profile might become asymmetrically deformed due to the effect of gravity. On the other hand, the liquid–liquid interface formed by two immiscible liquids can act as a lens refractive surface, and the shape of the refractive surface can be controlled by fluid pressure [8,9], electro-wetting [11], or dielectrophoretic effect [12,13]. A fluid pressure liquid lens is driving under a typical mechanism that pumping liquid in and out of the lens chamber which changes the curvature of the liquid-liquid interface, in turn, the focal length could be controlled [8,9]. In an electro-wetting lens, the contract angle on the chamber surface formed by the non-conductive liquid could be dynamitic controlled by applying different voltages [11,16]. In a dielectrophoretic lens, dielectric force is generated under an inhomogeneous electric field between low and high dielectric constant liquids, and therefore the curvature of the liquid–liquid interface will be deformed [12,13]. Electro-wetting devices and dielectrophoresis devices both use external voltage and they could be driven silently, but the Joule heating and microbubbles might arise for a long operating time. Nevertheless, two immiscible liquids with high transparency, equal density, and a large refractive index difference are considered to be ideal, but it is difficult to prepare liquids with the same density at any temperature due to thermal expansion. However, if the aperture size were designed to be sufficiently smaller than the capillary length, the surface tension would become the dominant force, and the effect of gravity would be negligible [8,10]. The capillary length, lc, is a characteristic length scale for a fluid subjected to gravity and surface tension and is given by

$$l_c = \sqrt{\frac{\sigma}{\left|\rho_{liquid1} - \rho_{liquid2}\right| g}}, \tag{1}$$

where $\sigma$ is surface tension, $\rho_{liquid1}$ and $\rho_{liquid2}$ are the liquid densities, and $g$ is the gravitational constant. When the lens aperture diameter, $d$, is sufficiently smaller than the capillary length ( $d < l_c$ ), gravity will be negligible. Therefore, the capillary length is a physical limitation that restricts the size of a liquid–liquid lens.

A method of fabricating a large-aperture variable focus lens by utilizing an elastic force to take the place of interfacial tension was reported, and a lens with a liquid–membrane–liquid (LML) structure was fabricated with this method [10]. This LML lens exhibited tunable behavior, shifting from a positive lens to a negative lens, and had acceptable optical performance when the membrane was sufficiently deformed. The elastic force gradually increased as the external pressure was increased, and therefore, it is presumable that, in the beginning of the deformation period, the deformation shape will be dominated by the force of gravity. This phenomenon mainly occurs in the region where the lens has low optical power region, which refers to the physical area that elastic force is not the dominate force and liquids are subjected to the gravitational acceleration. Because this region is between the regions of positive and negative optical power, it potentially makes some applications impossible, for example, adjustable ophthalmic eyeglasses or machine vision systems. Therefore, it is necessary to improve the variable focus lens in the region of low optical power, especially for an LML lens.

## 2. Design principle

The problem mentioned above occurs in the region of low optical power because the capillary length is not sufficiently longer than the lens aperture in this region. The lens aperture size should be much smaller than the capillary length to ensure sufficient lens performance [8,10]. In the example shown in Fig. 2 in literature [10], when the pair of liquids are assumed to be ultra-pure water and poly-dimethyl-siloxane (PDMS) liquid, if the lens aperture is 30 mm in diameter, the capillary should be longer than 80 mm, otherwise the lens will not perform well in the vertical orientation.

To overcome this problem, we propose distributing an in-plane pretension force on the elastic membrane, so that the membrane is stretched in the initial state. Thanks to the in-plane pretension force, a strong elastic force can be generated and, in principle, a sufficient capillary length could be achieved in the initial stage; as a result, the variable focus performance in the region of low optical power could be improved.

Large deflection of a membrane clamped at a circular boundary under in-plane pretension has been widely investigated [22,23]. Assuming a circular membrane with the same properties, like the thickness and radius under a uniform pressure and pretension, the axial deformation of the membrane is suppressed compared with one that is not subjected to pretension [23]. Physically, this is due to the additional pretension force in the radial direction, which changes the initial force of the radial equilibrium. In turn, the membrane deflection behavior is changed, because the function describing the axial displacement is related to the initial pretension force, and the elastic force has already yielded in the in-plane direction of the membrane.

To confirm the benefits of the pretension, a series of simulations of membrane deformation with and without a pretension force were conducted using the finite element method (FEM) with ANSYS software. The parameters were set as follows: the membrane was 30 mm in diameter and 0.1 mm in thickness with a clamped circular boundary, and as for the elastic properties, the Young's modulus was 5 MPa and Poisson's ratio was 0.45. The membrane was randomly divided into a mesh of 1425 elements. Candidate fluids were ultra-pure water (density 0.997 g/cm$^3$, refractive index 1.33) and PDMS liquid (density 0.975 g/cm$^3$, refractive index 1.40). The pretension force on the membrane was achieved by applying a 1 °C negative temperature difference with respect to a reference temperature of 20 °C at which the membrane's thermal expansion coefficient was determined, and the secant coefficient of thermal expansion was set to 0.004. By doing so, the pretension force will be distributed over the membrane. Two membrane models, one with a pretension force and one without, were constructed for comparison.

An elastic membrane, whose circular boundary is rigidly fixed, is model as radius a and thickness d, formed of a material of Young's modulus E, density ρ, and Poisson's ratio ν. When a uniform pressure P is applied to one surface of the disk, the deformation z = R(r) is denoted by the following polynomial:

$$R(r)=\frac{a^4P}{64D}\left\{\left(\frac{r}{a}\right)^4-2\left(\frac{r}{a}\right)^2+1\right\}, \tag{2}$$

where D denotes the bending rigidity, given by:

$$D = Ed^3 / 12(1-\nu^2). \tag{3}$$

However, the FEM simulation imitates the LML system in the vertical orientation, which the effect of gravity is regarded as being a maximum. Due to the density differences between two liquids, the membrane is suffered a linearly increased hydraulic pressure acts in a direction towards the smaller-density side, which is:

$$P_{hydraulic} = \left(\rho_{liquid1} - \rho_{liquid2}\right) \times g \times 2a, \tag{4}$$

Meanwhile, because the FEM imitates the in-plane pretention according to the thermal expansion phenomena, the thermal expansion $\varepsilon_{thermal}$ and thermal stress are:

$$\varepsilon_{thermal} = \alpha\left(T - T_{\mathrm{Re}f}\right), \tag{5}$$

$$\sigma_{thermal} = E\alpha\left(T - T_{\mathrm{Re}f}\right), \tag{6}$$

where $\alpha$ is the coefficient of thermal expansion, and $T - T_{\mathrm{Re}f}$ is the temperature change on the model, respectively. In general, the deflection on the membrane model is defined by multiple pressures by means of the uniform pressure, hydraulic pressure and the thermal stress, and this deformation analysis was conducted by FEM simulation.

The membrane model was meshed into elements, and the coordinates of the mesh elements were recorded according to the 3D deformation of the membrane. Distances between the locations of the maximum deflection on the membrane to the geometric center are plotted in the upper left graph in Fig. 1 against optical power. The optical power was deduced according to the maximum deflection on the membrane and the refractive indices of the two liquids, where only in this calculation the deflection was assumed to be spherical so as to deduce the lens power. In the vertical axis, a smaller scale of the shifted distance means the maximum deflection on the membrane is closer to the geometric center, and the deformation shape is closer to a symmetric shape. In the upper left graph of Fig. 1, the plot of the pretensioned membrane performed a smaller value compares to the no pretensioned membrane. For example, when 6.468 Pa and 36.468 Pa external pressure were loading on the no pretentioned membrane (lower left) and pretentioned membrane (lower right), respectively, the maximum deformation degree were similar but the deformation shape of the pretensioned membrane was much closer to a symmetric shape. Two snapshots of the deformed membrane models were shown in the lower of Fig. 1. Moreover, a range of power from 0.03 to 0.26 could be exhibited by the pretensioned model because the displacement was suppressed by the initial in-plane elastic force. The optical path lengths (OPLs) of the deformed surface were calculated based on the 3D deformation and the refractive indices of the liquids. Then, the wavefront surface defined by the OPLs was fitted to a spherical surface, and the root mean square error (RMSE) was acquired from the fitting results. The upper right graph in Fig. 1 shows the comparison result of wavefront errors in terms of RMSE values. In brief, the proposed lens should achieve better performance by means of symmetrical deformations and lower wavefront errors because of the in-plane pretension of the membrane.

#214843 - $15.00 USD Received 26 Jun 2014; revised 27 Jul 2014; accepted 27 Jul 2014; published 5 Aug 2014

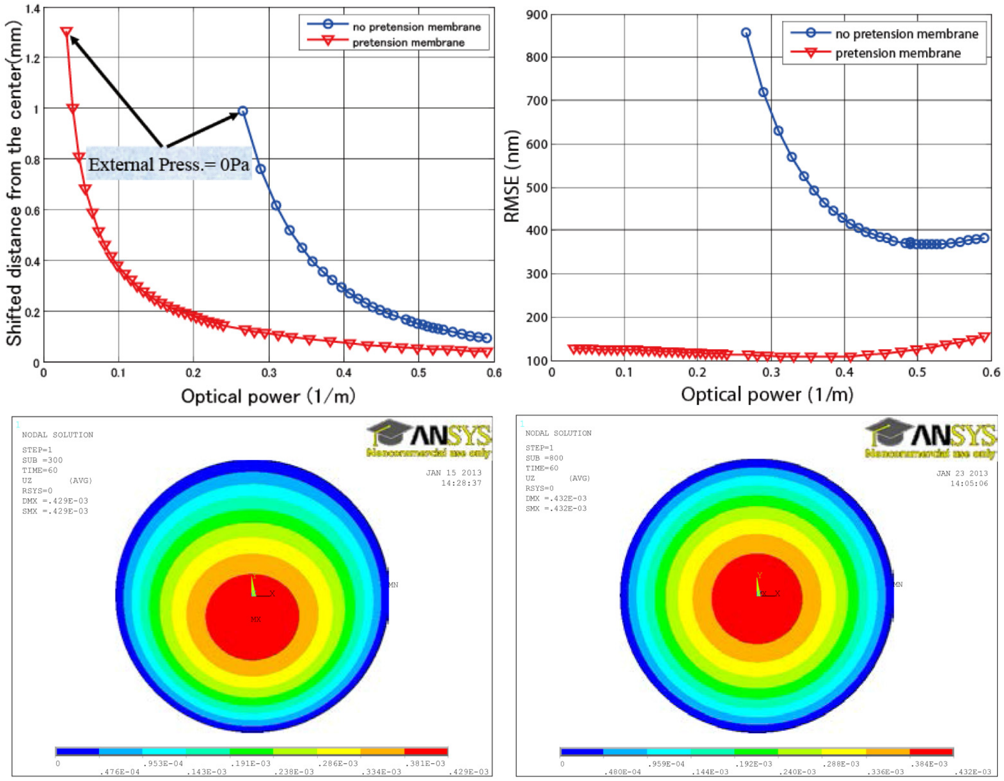


Fig. 1. A comparison of the membrane with in-plane pretension (red line) and without pretension (blue line) was shown in the upper. The pretension model exhibited better symmetrical deformation, as indicated by the small shift distance (upper left), and lower wavefront errors, as indicated by the small RMS error (upper right). Two snapshots of the deformed membrane models were shown in the lower, when 6.468 Pa and 36.468 Pa external pressure were loading on the no pretentioned membrane (lower left) and pretentioned membrane (lower right), respectively.

## 3. Experiment and discussion

A prototype variable focus lens was constructed, and the membrane was prepared by distributing a homogenous in-plane pretension force. The upper image of Fig. 2 shows a cross-sectional view of the structure of the variable focus lens and the membrane. An elastic membrane was bonded to Frame A smoothly without stress. In section 2, the in-plane pretension on the membrane was modeled by the thermal expansion in simulation, but in actual experiment we built it with another fabrication method. In order to distribute an in-plane pretension force homogenously, Frame B was introduced and designed with a bulged circular inner ring. When the membrane was clipped between Frame A and Frame B, it was pushed up, thus being stretched, causing a uniform pretension force to act in the in-plane direction of the membrane. The three parts were fixed at the center of the lens device, and O-rings were used to prevent liquid leakage. The two chambers were infused with two different liquids. If one of the liquids can be made to freely flow into and out of its chamber, while the end of tube of the other chamber is locked, the lens can shift its power dynamically from positive to negative by means of a syringe.

#214843 - $15.00 USD Received 26 Jun 2014; revised 27 Jul 2014; accepted 27 Jul 2014; published 5 Aug 2014
 

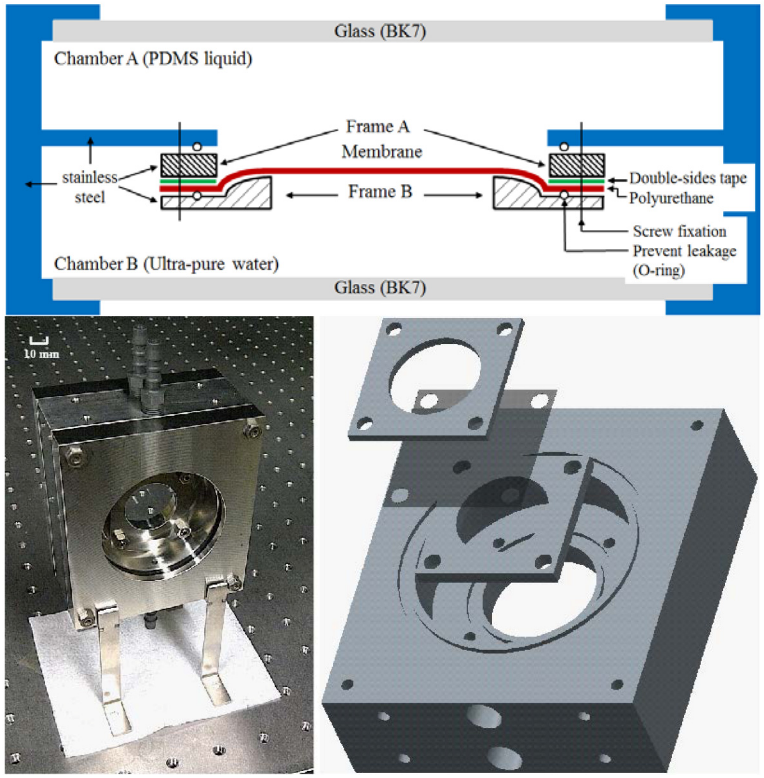


Fig. 2. (upper) A cross-sectional view of the structure of the variable focus lens and the membrane. The membrane was bonded to Frame A beforehand and was clamped by Frame B, which had an inner circular bugle so as to push the membrane upward, and the three parts were fixed together. (lower) A photograph of the LML system and an exploded view of the model.

Following the above fabrication procedure, a square piece of membrane with a thickness of 0.1 mm and a size of 40 mm × 40 mm was prepared and clamped by Frames A and B having outer sizes of 40 mm × 40 mm. Because Frame B had to be designed with an inner circular bugle, the aperture of the circular hole was cut to 26 mm in diameter. Nevertheless, this size of variable focus lens could still be called a large-aperture variable focus lens. A photograph of the LML system and an exploded view of the model are shown in lower of Fig. 2. The device were made by stainless steel and the glass windows were made from BK7 (φ80 mm, thickness 8 mm, OPB-80C08-1-5, Sigma Koki), the size of the whole lens system was 100 mm × 90 mm × 52 mm. O-rings were inserted between the contact surfaces of the parts. The containers of chambers were designed with 60 mm in diameter with 7 mm thickness for chamber A and 15 mm thickness for chamber B. Polyurethane was used to form the membrane sheet, so as to ensure compatibility with the PDMS liquid. The liquids should have high transparency, the same density, and a large refractive index difference. Even though certain additives could be added to one of the liquids to match their densities, a density difference will appear again if the surrounding environment is changed, such as thermal expansion due to a changing temperature. Hence, a certain density difference was admitted. The selected liquid candidates were ultra-pure water and PDMS liquid. The following experiments were conducted at a temperature of 20 °C, at which the density difference was 22 $kg/m^3$. The effect of gravity is regarded as being maximum when the liquid lens is placed in the vertical orientation. A pressure that linearly increases from top to bottom according to hydraulic pressure acts in a direction towards the smaller-density side. Initially, the membrane will be oriented in the vertical direction and will be subjected to a resultant force from a uniform pretension force in the radial direction and a non-uniform hydraulic force in the axial direction.

There was a slight deflection of the membrane when the liquid lens was placed in the vertical direction and the liquids were infused, but without external pressure, because of the force due to the difference of the densities. The degree of deflection of the membrane was too small to measure directly; and therefore, we measured the wavefront behavior of the liquid lens when it was assumed to act as an infinite-focal-length lens [24]. Figure 3 shows a schematic illustration in the upper and photograph of the measurement setup in the lower. A high-speed camera (Phantom V4.2, Vision Research, Inc.) mounted to a Shack-Hartmann (SH) wavefront sensor (Omi-22-200, SpotOptics) was used. Because the aperture size of the SH lens array was 2.5 mm, and the liquid lens aperture was 26 mm in diameter, a beam expander (BE60, custom-designed by SpotOptics) was placed in reverse orientation to match the aperture sizes. A parallel beam was sent from a collimator (CAL60, SpotOptics) and passed through the test lens, during which the beam was partially blocked by the lens' frame. The SH sensor needs a reference wavefront. First, a collimated beam of light coming from a collimator and passing through the beam expander before falling on the SH sensor was captured as a reference image. After that, the test lens was placed between the collimator and the beam expander. Ultra-pure water and PDMS liquid were infused into the two chambers at the same time to the same height, and no external pressure was loaded. The wavefront profile was reshaped based on the refractive index difference of the liquids and the degree of deflection of the membrane. The wavefront was recorded and compared with the reference image, as shown in Fig. 4.

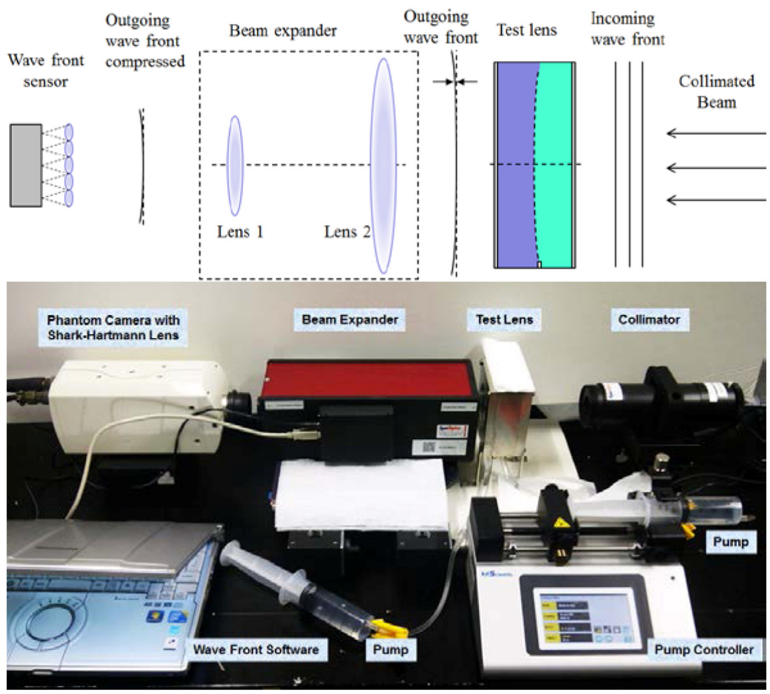


Fig. 3. Illustration of the wavefront error measurement when the lens had an infinite focal length (upper), and a photograph of the experimental setup (lower).

A peak-to-valley height (P-V) of 478 nm and a root-mean-square (RMS) wavefront error of 105.1 nm were measured. The P-V height was worse than a Rayleigh's quarterwave rule, and the RMS was higher than wavelength/14, the Marechal criterion [25]. In the wavefront profile, the peak and valley deviations were found in the center (blue zone) and the upper right corner (red zone). The deviation in upper right corner (red zone) might result from the fabrication procedure, which was conducted in manual, because the circular boundary condition could not be ensured in a high precision. To understand the membrane's deflection, the blue zone in the center was regarded as the maximum-deformation area, and the degree of membrane deformation was estimated to be −3.90 µm, which is quite a small error for a flat membrane.

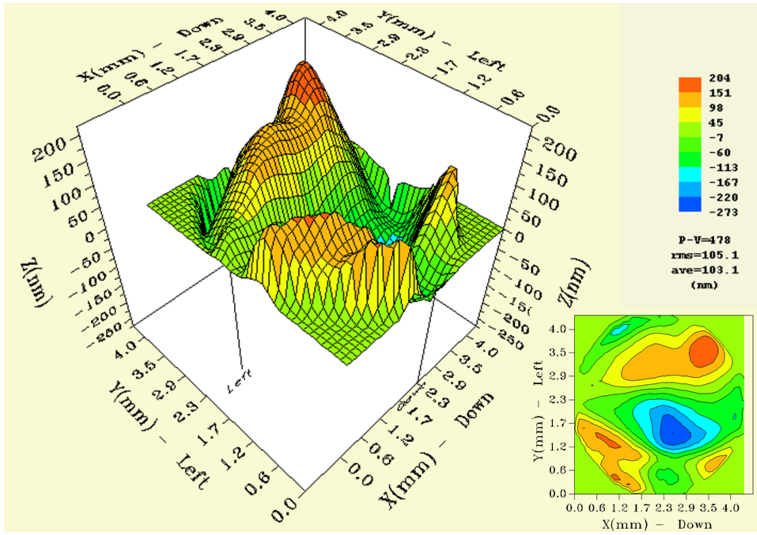


Fig. 4. Wavefront error with an infinite focal length.

Furthermore, wavefront error profiles were measured when the test lens was configured with four focal lengths of 500, 600, 700 and 800 mm. A light pipe homogenizer was connected to a metal halide lamp (IMH-250, Sigma Koki), and the light was passed through a pinhole (100 µm in diameter); these two devices were employed to replace the collimator. During this measurement, the distance between the pinhole and the test lens was adjusted according to the focal length of the test lens, so that the outgoing light from the test lens was a parallel beam. The P-V and RMS error results are listed in Table 1. The P-V values were high. The primary reason for this was found to be due to the unsuppressed deflection on the boundary area when increased the external pressure. The minimum RMS error was 149.1 nm when the focal length was 800 mm. Although the maximum RMS error was 266.4 nm when the focal length was 700 mm, this is considered to be adequate performance for a liquid lens with such a large aperture. Furthermore, the boundary condition was critical for the lens behavior, so that the deformation could be confined within a circular boundary condition. The fabrication procedure described above was performed manually. If a better processing technology were employed to improve the precision of the circular boundary, it should be possible to fabricate a lens with even better performance. To evaluate the lens imaging performance, we recorded an image of a target (USAF 1951 chart, Edmund) through the LML lens. The target was place 200 mm in front of the test lens and a COMS camera (5D Mark II zoom with 21.1M pixels) was behind. Figure 5 shows the recorded image when the lens focal length was 500 mm.

**Table 1. Wavefront error performance (P-V and RMS) with different focal lengths.**

| Focal length [mm] | Peak-to-Valley [nm] | Root-Mean-Square [nm] |
|---|---|---|
| infinity | 478 | 105.1 |
| 800 | 884 | 149.1 |
| 700 | 1571 | 266.4 |
| 600 | 1225 | 241.3 |
| 500 | 1305 | 236.4 |

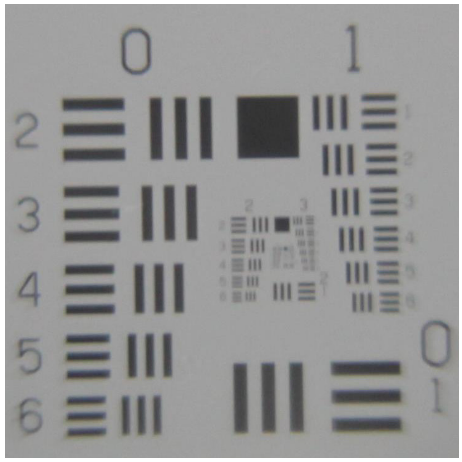

Fig. 5. An image was taken from the LML lens prototype when its focal length was 500 mm.

## 4. Conclusion

In summary, we studied the deflection of an elastic membrane and proposed the use of an elastic force to take the place of surface tension so that a variable focus lens with a large aperture could be realized. However, when the lens is set in its low-optical-power region, the membrane badly deforms into an asymmetrical shape because the membrane is not sufficiently deformed. To solve this problem, we proposed distributing an in-plane pretension force on the membrane so that a strong elastic force could be generated, which would, in principle, achieve sufficient capillary length in the initial stage and, in turn, a sufficient capillary length in the low-optical-power region of the lens. Improved performance was confirmed by conducting a comparison between membranes with and without in-plane pretension loading by using the finite element method. A prototype variable focus lens with a 26 mm-diameter aperture was fabricated, and the behavior of the lens in the low-optical-power region was measured by using a Shack-Hartmann sensor. Thanks to the in-plane pretension force, the lens could achieve an infinite focal length with a root-mean-square wavefront error of 105.1 nm. This fabrication method can potentially be used for fabricating a much larger variable focus lens. It will be possible to improve the lens performance by employing a high-precision fabrication procedure, and a variety of applications that might utilize the low-optical-power region of the lens will become possible, such as adjustable ophthalmic eyeglasses, zooming and focusing vision systems, etc.

#214843 - $15.00 USD Received 26 Jun 2014; revised 27 Jul 2014; accepted 27 Jul 2014; published 5 Aug 2014